

Rotation and shape changes in ^{151}Tb and ^{196}Pb : Probes of nuclear structure and tunneling process in warm nuclei. I. Experimental analysis

S. Leoni,^{1,2} G. Benzoni,² N. Blasi,² A. Bracco,^{1,2} F. Camera,^{1,2} A. Corsi,^{1,2} F. C. L. Crespi,^{1,2} P. Mason,^{1,*} B. Million,² D. Montanari,^{1,2} M. Pignanelli,^{1,2} E. Vigezzi,² O. Wieland,² M. Matsuo,³ Y. R. Shimizu,⁴ D. Curien,⁵ G. Duchêne,⁵ J. Robin,⁵ P. Bednarczyk,⁶ M. Castoldi,⁷ B. Herskind,⁸ M. Kmiecik,⁶ A. Maj,⁶ W. Meczynski,⁶ J. Styczen,⁶ M. Zieblinski,⁶ K. Zuber,⁶ and A. Zucchiatti⁷

¹*Dipartimento di Fisica, Università di Milano, via Celoria 16, I-20133 Milano, Italy*

²*INFN, Sezione di Milano, via Celoria 16, I-20133 Milano, Italy*

³*Graduate School of Science and Technology, Niigata University, Niigata 950-2181, Japan*

⁴*Department of Physics, Kyushu University, 6-10-1 Hakozaeki, Higashi-ku, Fukuoka 812-8581, Japan*

⁵*IPHC-DRS, ULP, CNRS, IN2P3, 23 rue du Loess, F-67037 Strasbourg, France*

⁶*The Niewodniczanski Institute of Nuclear Physics, Polish Academy of Sciences, PL-31-342 Krakow, Poland*

⁷*INFN, Sezione di Genova, via Dodecaneso 33, I-16146 Genova, Italy*

⁸*The Niels Bohr Institute, Blegdamsvej 15–17, DK-2100 Copenhagen, Denmark*

(Received 30 January 2009; revised manuscript received 7 May 2009; published 10 June 2009)

The γ decay associated with the warm rotation of the superdeformed nuclei ^{151}Tb and ^{196}Pb has been measured with the Euroball IV array. Several experimental quantities are presented, putting strong constraints on the decay dynamics in the superdeformed well. The data are successfully reproduced using a Monte Carlo simulation of the γ decay based on microscopically calculated energy levels, $E2$ decay probabilities, collective mass parameters, and potential energy barriers between the wells associated with normal and super deformation. This allows one to test the basic ingredients of the physical process, such as the strength of the two-body residual interaction and the potential barriers as a function of spin and excitation energy. We also show that the data probe the $E1$ strength function, indicating an enhancement around 1–2 MeV γ rays, which might be related to octupole vibrations.

DOI: [10.1103/PhysRevC.79.064306](https://doi.org/10.1103/PhysRevC.79.064306)

PACS number(s): 21.10.Re, 23.20.Lv, 25.70.Gh, 27.70.+q

I. INTRODUCTION

The existence of superdeformed (SD) rotational bands, extending over a long series of quadrupole transitions and finally decaying toward spherical or low deformation states, represents a striking manifestation of shape coexistence in nuclei. In many cases, several discrete SD bands have been discovered in the same nucleus [1], and the study of quasi-continuum (QC) spectra has demonstrated that rotational correlations associated with large deformation persist also when the nucleus is warm, i.e., at higher values of U [2,3], the excitation energy above the yrast band. This is similar to what has been observed in normal deformed (ND) systems [4–7].

In both SD and ND nuclei, as U increases, the two-body residual interaction starts to mix the single-particle levels on which the rotational bands are based, resulting in the compound nucleus states. This produces a gradual transition between order and chaos, which has been systematically studied in the past within the interacting cranked shell model of Refs. [8–11]. The character of quadrupole transitions is also affected by the residual interaction, leading to the phenomenon of rotational damping [12], by which the $E2$ transitions between mixed states acquire a width affecting the experimental QC spectra [4,5].

The study of the warm rotation, carried out in great detail in ND nuclei [4,7,13–18], is particularly challenging, both

experimentally and theoretically, in very elongated systems. Experimentally, high selectivity and high statistics are in fact needed, in order to focus on the small fraction of the γ decay (\approx few %) which is finally trapped into the SD well. Although this investigation is very complex, the topic is particularly appealing because it gives insight into not only the effects beyond the mean field, but also the important physical mechanisms underlying quantum tunneling at the onset of the chaotic region. This is relevant also in connection with the search for hyperdeformed shapes [19].

Theoretically, the study of the warm rotation requires a deep understanding of nuclear structure properties beyond mean field and a detailed description of the γ -decay flow, from the chaotic compound nucleus at high angular momentum to the cold, ordered region close to the yrast line [13]. This is based on the competition between statistical dipole ($E1$) and collective quadrupole ($E2$) transitions, which depends on the level densities and on the $E1$ and $E2$ strength functions over a wide range of energies. In addition, in the case of SD nuclei, one has to consider the coupling between excited SD and ND configurations, which is usually described as a tunneling process through the potential barriers separating the two wells [20,21]. For these reasons, the γ decay in the SD regime is poorly known: up to now only partial experimental information is available for a few SD nuclei [2,3,22–24], and the interpretation of the data is based on rather schematic models [2,22,24] or depends on several parameters [3,23].

In this work, we present a detailed study of the population and decay of the warm SD nuclei ^{151}Tb and ^{196}Pb , representative of the mass regions $A = 150$ and $A = 190$, in which

*Present address: INFN Laboratori Nazionali di Legnaro, Viale dell'Università 2, I-35020 Legnaro (PD), Italy.

discrete SD bands are known to have remarkably different properties. We shall see that these differences extend also to the case of quasi-continuum spectra and that they can be well accounted for within the same phenomenological model. As reported in Ref. [25], we have been able for the first time to obtain a series of independent observables that provide strong experimental constraints on the decay dynamics of excited SD nuclei, populated by neutron evaporation following fusion reactions. These observables are the intensities and fluctuations in the number of counts, measured as a function of spin, associated with different structures observed in QC γ -coincidence spectra, with appropriate gating conditions. A key point of the analysis is the comparison of the experimental results with a newly developed Monte Carlo simulation of the decay flow, which is based on the microscopic cranked shell model of Refs. [10,11] and on the microscopic barriers of Ref. [26]. This has several advantages: (i) the number of free parameters is limited, (ii) the inclusion of individual quantal states allows one to compare the fluctuations of simulated spectra with experiment, and (iii) detailed nuclear structure effects can be considered.

We anticipate that such a detailed study of the γ -decay flow in the quasi-continuum provides a tool for probing the $E1$ strength below particle emission, in particular the low energy tail down to ≈ 1 – 2 MeV. This is a topic of general interest in nuclear physics, also in connection with reaction studies and astrophysics, which is presently being widely investigated also in exotic nuclei [27–30]. Furthermore, the study of warm rotation provides specific information on the strength of the two-body residual interaction and on the potential barriers as a function of spin and excitation energy.

In this first part of the paper, we discuss in detail the experiments (Sec. II) and the analysis of quasi-continuum spectra (Sec. III). In Sec. IV we give the interpretation of the experimental results based on the Monte Carlo simulation of γ decay in the SD well, while the sensitivity to specific aspects of the physical process, such as the strength of the two-body residual interaction and the potential barriers between SD and ND states, will be discussed in Sec. V. For a detailed description of the Monte Carlo simulation and the ingredients of the theoretical model, we refer the reader to Part II [31].

II. THE EXPERIMENT

The experiments were performed at the Vivitron accelerator in Strasbourg, France, with the Euroball IV array [32,33]. The reactions used were $^{130}\text{Te}(^{27}\text{Al}, 6n)^{151}\text{Tb}$ (at 155 MeV) and $^{170}\text{Er}(^{30}\text{Si}, 4n)^{196}\text{Pb}$ (at 148 MeV). In both cases, a stack of two self-supporting targets (with a total thickness of ≈ 1 and 1.2 mg/cm², respectively) were employed. In the Tb case, the full Ge ball was used, while in the Pb experiment the low efficiency Ge detectors were replaced by eight large volume BaF₂ scintillators to measure high energy γ rays. In both cases, the γ multiplicity was measured with an InnerBall of bismuth germanate (BGO) detectors. A total of $\approx 9 \times 10^9$ and 2×10^8 four- and three-fold events and higher were collected, respectively. The nuclei of interest, ^{151}Tb and ^{196}Pb , were populated at the level of $\approx 70\%$ and $\approx 20\%$, respectively, ^{195}Pb being in the latter case the most intense reaction channel.

The nuclei ^{151}Tb and ^{196}Pb have been previously investigated in detail by discrete γ spectroscopy. They both show a low deformation configuration [here named “normal deformed” (ND)], characterized by very little collectivity [34–37]. At high spins, both ^{151}Tb and ^{196}Pb show a well-developed superdeformed minimum: up to 10 SD excited bands have been found in ^{151}Tb [38] and 4 in ^{196}Pb [1,39], with intensities down to less than 10% and 30% of the corresponding SD yrast, which collects $\approx 2\%$ and $\approx 1.3\%$ of the population of the nucleus of interest, respectively (see discussion in Sec. IV). In both nuclei, discrete transitions linking the SD yrast band to ND configurations were identified, therefore making it possible to assign the spin and excitation energy of the SD yrast [40,41]. In the case of ^{151}Tb , the most recent spin assignment is found to be 2 spin units higher than previously reported in Ref. [1].

The topic of this paper is the analysis of quasi-continuum one-dimensional (1D) and two-dimensional (2D) γ -coincidence spectra, which provide information on the unresolved excited SD rotational bands [25]. This allows us to study the properties of the γ -decay flow at the onset of the transition between order and chaos in the atomic nucleus [4]. For this purpose, the two data sets have been sorted into a number of γ - γ matrices in coincidence with low-lying ND transitions of the isotope of interest, namely, $E_\gamma = 268.4, 597.4, 604.5,$ and 615.9 keV in ^{151}Tb (corresponding to the transitions $31/2^+ \rightarrow 29/2^+, 19/2^+ \rightarrow 15/2^+, 15/2^- \rightarrow 11/2^-,$ and $19/2^- \rightarrow 15/2^-$) and $E_\gamma = 468, 502,$ and 959 keV (corresponding to the transitions $15^- \rightarrow 14^+, 16^- \rightarrow 15^-,$ and $14^+ \rightarrow 12^+$) in ^{196}Pb . These matrices have been named “Total,” at variance with the spectra sorted in coincidence with the cleanest transitions of the SD yrast band of each nucleus (named “SD-gated”). In addition, the so-called rotational planes (ROT-planes) were sorted [42]. These are matrices with the triple coincidence requirement $x + y = 2z \pm \delta/2$, where $x, y,$ and z are the energies of the γ rays and δ is the thickness of the plane, which in the present case has been chosen to be ≈ 20 keV, allowing for some irregularities in the rotational energy sequence. In these spectra, the sensitivity to rotational correlations among discrete bands in the γ cascades is largely enhanced as compared to a background of fragmented/uncorrelated decays, since rotational correlations extending at least over three steps are selected (see Fig. 1 for a schematic illustration of the rotational correlation patterns in both a γ - γ spectrum and a rotational plane, as follows from a regular rotational decay). In all sorted matrices a condition on high-fold events ($F \geq 25$ for ^{151}Tb and $F \geq 10$ for ^{196}Pb) was imposed, to better focus on high-multiplicity cascades. For each matrix, the major part of the background has been removed by subtracting the ungated spectrum scaled by a factor corresponding to the peak-to-total (P/T) of the gating transitions (i.e., to the ratio of the peak intensity relative to the total intensity measured in the energy interval of the gate). P/T is of the order of 0.4 (0.2) in ^{151}Tb (^{196}Pb), in the case of the ND low-lying gating transitions. In the case of the yrast SD-gated spectra, the P/T value was estimated to be less than 0.02. In addition, the COR procedure [43] has been applied, with a reduction factor of ≈ 0.8 and 0.9 for the Total matrices, ≈ 0.4 and 0.3 for the ROT-planes, and ≈ 0.5 and 0.75 for the

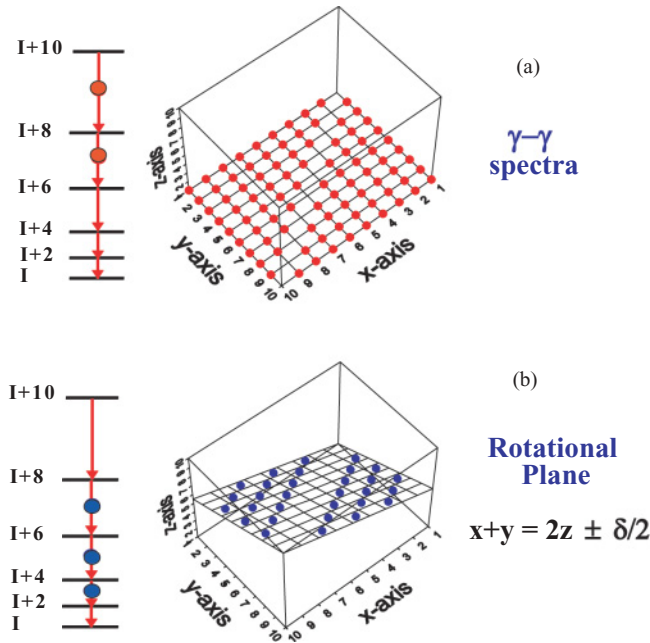


FIG. 1. (Color online) Schematic illustration of the rotational correlation patterns following a regular rotational decay, for (a) a γ - γ coincidence spectrum and (b) the rotational plane defined by the equation $x + y = 2z \pm \delta/2$, where x , y , and z are the energies of the γ rays, and δ is the thickness of the plane (see text for details). The combination of coincident γ rays selected by the two spectra are indicated by circles in the rotational cascades shown in the left-hand side of each figure.

SD-gated spectra of ^{151}Tb and ^{196}Pb (according to the method discussed in Ref. [5]). The latter treatment enhances the ridge structures and removes the uncorrelated background that may still be present after the previous background subtraction.

In addition to the 2D matrices, 1D spectra, double gated on the cleanest transitions of the SD yrast band of ^{151}Tb and ^{196}Pb , have been sorted. The spectra have been subtracted from the background and unfolded using the unfolding procedure provided by the RADWARE package [44]. The $E1$ component in coincidence with the SD yrast band has also been removed, as previously done in the analysis of the SD nucleus ^{143}Eu [23]. The remaining spectra should therefore contain pure $E2$ contributions, except for possible contaminants of $M1$ nature, not investigated in the present analysis but clearly observed at low transition energies in neighboring nuclei of both mass regions [3,45,46].

The left-hand columns of Figs. 2 and 3 show the experimental γ spectra of ^{151}Tb and ^{196}Pb , respectively. In both figures, panels (a), (c), and (e) give examples of cuts perpendicular to the main diagonal of the 2D γ -coincidence spectra, for the wide spin intervals ≈ 48 – $56\hbar$ (^{151}Tb) and ≈ 20 – $34\hbar$ (^{196}Pb). Panels (a) refer to Total matrices, (c) to the ROT-planes, and (e) to the SD-gated spectra. In all cases, ridge structures are clearly visible, with a spacing between the two most inner ridges equal to $2\Delta E_\gamma = 8\hbar^2/\mathfrak{I}^{(2)} \approx 100$ and 80 keV in ^{151}Tb and ^{196}Pb , respectively, where $\mathfrak{I}^{(2)}$ is the moment of inertia of the SD yrast band in each nucleus. The intensities of the known ND and SD discrete peaks, which were subtracted from

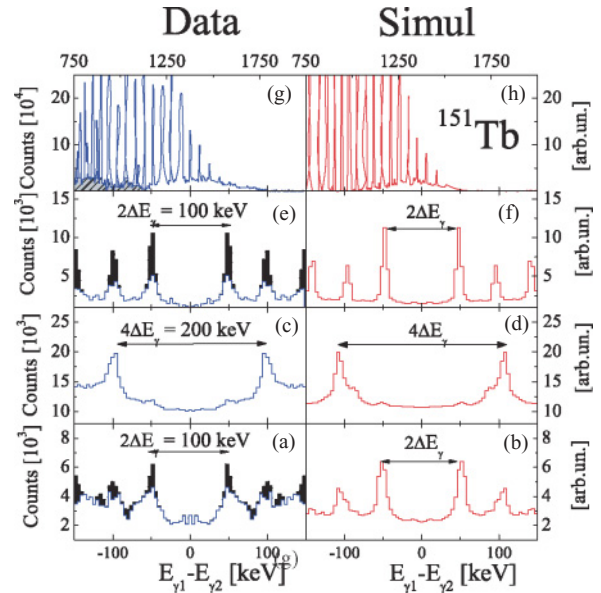


FIG. 2. (Color online) Experimental and simulated spectra of ^{151}Tb . Panels (a)–(f) show projections perpendicular to the main diagonal of the Total γ - γ coincidence matrices [(a),(b)], of the rotational planes [(c),(d)], and of the SD-gated spectra [(e),(f)], corresponding in the data to the spin interval 48 – $56\hbar$. The dark areas in panels (a) and (e) correspond to the intensity of known ND and SD discrete peaks subtracted from the spectra by the RADWARE package [44]. Panels (g) and (h) show one-dimensional $E2$ quasi-continuum spectra gated by the SD yrast; the shaded area in the experimental spectrum corresponds to the region where contaminants from $M1$'s are expected, as observed in neighboring nuclei (see text for details).

the Total and SD-gated matrices by means of the RADWARE package before performing any further analysis of the data, are

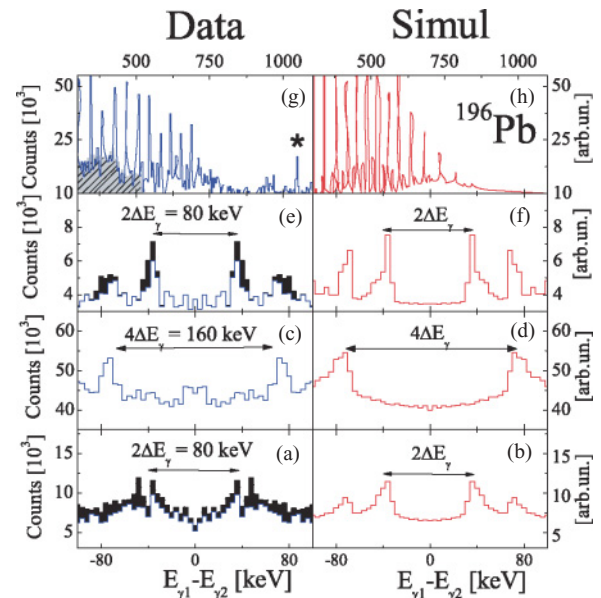


FIG. 3. (Color online) Same as Fig. 2, but for ^{196}Pb . In this case, the projections of the 2D matrices correspond to the spin interval 20 – $34\hbar$ (see text for details).

indicated by dark areas. For the SD states, the only significant contribution comes from the SD yrast. For the ROT-planes spectra, the cuts have been instead obtained by projecting the 2D spectra in between the SD yrast peaks, therefore resulting in event distributions free from strong contaminants from discrete peaks. In this case, the most inner ridge corresponds to the second ridge in the Total and SD-gated matrices, and its spacing is therefore twice as large. The top panel (g) of both figures gives the one-dimensional quasi-continuum spectra double gated by the SD-yrast band of ^{151}Tb and ^{196}Pb (with the energy scale on the top axis). In each spectrum, the SD yrast is clearly visible; in the case of ^{196}Pb , the strong peak at $E_\gamma = 1049$ keV (marked by a star) is the $2^+ \rightarrow 0^+$ ground state transition in coincidence with the SD yrast band. The shaded areas at low energies (i.e., below ≈ 1100 and ≈ 500 keV in ^{151}Tb and ^{196}Pb , respectively) may be attributed to possible $M1$ contaminants, as observed in neighboring nuclei [3,45,46]. The broad bump above ≈ 1100 and 500 keV in ^{151}Tb and ^{196}Pb , respectively, is made mostly of unresolved $E2$ transitions, which we call the $E2$ quasi-continuum ($E2$ QC) hereafter.

The right columns of Figs. 2 and 3 show the corresponding simulated spectra of ^{151}Tb and ^{196}Pb , obtained by the Monte Carlo simulation MONTESTELLA (discussed in Sec. IV).

III. ANALYSIS OF QUASI-CONTINUUM SPECTRA

The experimental data have been analyzed in terms of (i) intensities of the five SD components observed in the γ -coincidence data: the SD yrast, the 1st ridge, the 2nd ridge, the SD-gated 1st ridge and the SD-gated $E2$ quasi-continuum, and (ii) fluctuations of the event distributions of the Total, rotational planes, and SD-gated ridge structures, giving the effective number of discrete excited bands populating the specific ridge structure [5]. In this way, eight experimental observables are obtained, providing strong constraints on the dynamics of the decay flow in the SD well [25].

A. Intensity analysis

First, the intensity pattern of the SD yrast band has been evaluated starting from the Total matrices gated on the ND low spin transitions which select the nucleus of interest (see previous discussion). This ensures a proper estimate of the population pattern, limiting the bias due to direct gating on the SD yrast transitions. The SD yrast bands of ^{151}Tb and ^{196}Pb are found to collect $\approx 2\%$ and $\approx 1.3\%$ of the population of the corresponding reaction channel. Their intensities, normalized to 100% in the low spin part of the plateau region (i.e., $I \leq 50\hbar$ in ^{151}Tb and $I \leq 20\hbar$ in ^{196}Pb), are shown as a function of spin in panels (a) and (b) of Fig. 4. For ^{151}Tb , we adopted the recent spin assignment given in Ref. [40], which is $2\hbar$ higher than that previously used in Ref. [25]; for ^{196}Pb , we followed Ref. [41].

The intensities of the various quasi-continuum components (extracted from the data of Figs. 2 and 3), evaluated relative to the SD yrast, are shown by symbols in Fig. 4. In all cases, the intensities are given as a function of spin, following the spin assignment of the SD yrast, as also discussed in connection

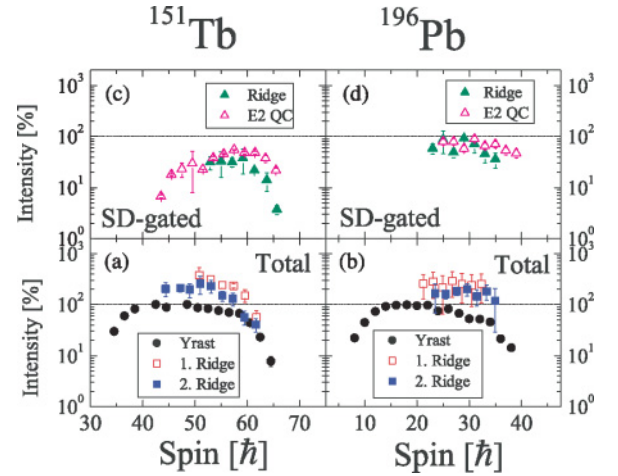


FIG. 4. (Color online) Population of the excited rotational bands in the SD well of ^{151}Tb and ^{196}Pb , normalized with respect to the SD yrast intensity at the plateau [full circles in panels (a) and (b)]. The intensities of the 1st and 2nd ridge are given in panels (a) and (b) by open and full squares. Panels (c) and (d) show by full and open triangles the population of the SD-gated 1st ridge and SD-gated $E2$ QC, respectively.

with Figs. 17 and 18 of Part II [31]. For the SD-gated quantities [Figs. 4(c) and 4(d)], the measured intensities at the highest spins have been reduced by a correction factor R_{yrast} : this takes care of the bias due to the gating on high spin transitions of the SD yrast, which causes an artificial enhancement of the intensities of the SD quasi-continuum structures. This factor is defined as the ratio between the intensity of the SD yrast observed in the SD gated spectra and in the ND gated ones, as shown in Figs. 5(a) and 5(b) for ^{151}Tb and ^{196}Pb . R_{yrast} is found to be relevant for the highest spin data (i.e., above 50 and 25 \hbar ,

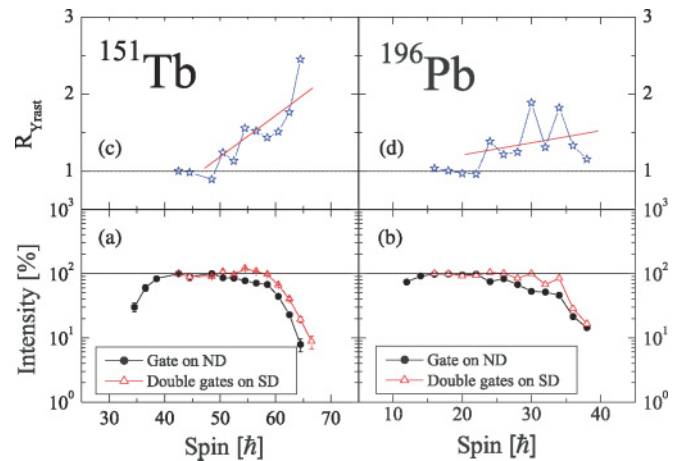


FIG. 5. (Color online) The bottom panels illustrate the effect of gating on transitions belonging to the SD yrast on the intensity pattern of SD yrast band of ^{151}Tb (a) and ^{196}Pb (b): circles refer to the SD yrast intensity obtained from the Total matrices (namely, sorted in coincidence with ND transitions), while triangles correspond to the analysis on the SD-gated spectra. Panels (c) and (d) give by stars the correction factor R_{yrast} and the corresponding linear interpolations, used to correct the data (see text for details).

respectively), resulting in a reduction of the intensities up to ≈ 1.5 – 2 for ^{151}Tb and ≈ 1.4 for ^{196}Pb , as shown in Figs. 5(c) and 5(d).

In both ^{151}Tb and ^{196}Pb nuclei, the total intensities of the 1st and 2nd ridge [Figs. 4(a) and 4(b)] are found to be up to three times larger than the population of the SD yrast at the plateau: this indicates the existence of several discrete unresolved SD bands that do not feed the SD yrast band, but decay into the low deformation minimum, as previously observed in the SD nucleus ^{143}Eu [2]. The results of the more selective analysis of 1D and 2D spectra in direct coincidence with the SD yrast [Figs. 4(c) and 4(d)] indicate that the intensity of the 1st ridge in coincidence with the SD yrast represents only a fraction of the yrast intensity, corresponding at most to 40% and 80% of the SD yrast intensity at spin $I \approx 55\hbar$ in ^{151}Tb and $\approx 25\hbar$ in ^{196}Pb . This means that for both nuclei, the SD yrast receives an important contribution from fragmented/damped bands at higher excitation energies, where rotational damping is expected to play a key role [4], as evidenced by the analysis of the $E2$ quasi-continuum [open symbols in Figs. 4(c) and 4(d)]. We note that, in this analysis, below spin ≈ 48 and $32\hbar$, in ^{151}Tb and ^{196}Pb , the data may be partially contaminated by $M1$'s (shaded areas in Figs. 2 and 3). As shown by symbols in Fig. 6, the intensity of the SD-gated ridges accounts for almost the entire $E2$ strength only for spins lower than $60\hbar$ in ^{151}Tb and $30\hbar$ in ^{196}Pb , corresponding roughly to the end of the plateau regions of the SD yrast. At higher spins, the ridge intensity drops to less than half of the $E2$ QC, indicating that most of the feeding of the yrast comes from damped bands.

The present results differ from the peculiar case of ^{194}Hg , where exceptionally narrow (≈ 10 keV) ridges have been observed in coincidence with the SD yrast, exhausting nearly all $E2$ decay strength and collecting the population of an extremely large number of discrete bands (≥ 100). This has been interpreted as an example of an ergodic nuclear system [24]. In the present work, the ridge structures in ^{151}Tb are found to be much wider, being of the order of 20 keV in the Total matrix and 16 keV in the SD-gated one, similar to the values previously reported in the analysis of both ND and SD nuclei [2,4]. In the case of ^{196}Pb , as shown in Fig. 7, rather wide structures are again observed in the Total matrix, while

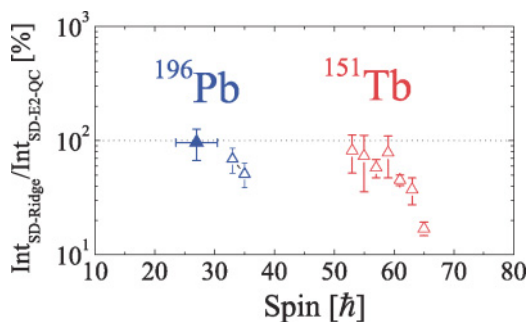


FIG. 6. (Color online) Ratio between the intensities of the SD-gated ridge and SD-gated $E2$ quasi-continuum [shown in Figs. 4(c) and 4(d)] for ^{151}Tb and ^{196}Pb . For ^{196}Pb , the filled triangle gives the average over the region where possible $M1$ contaminants are expected (see text for details).

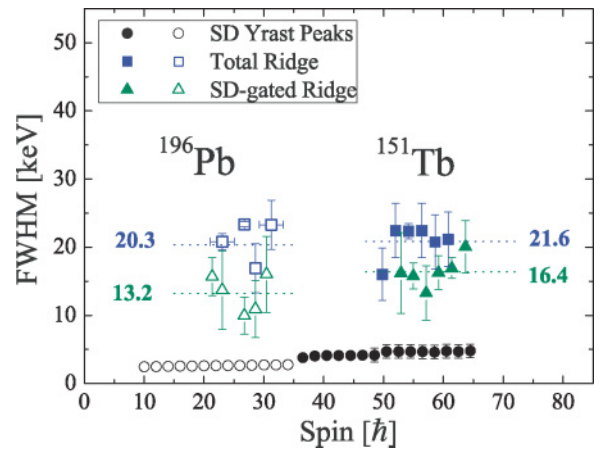


FIG. 7. (Color online) FWHM of the Total (squares) and SD-gated (triangle) experimental ridge structures compared with the width of the peaks of the SD yrast band (circles), for ^{151}Tb (full symbols) and ^{196}Pb (open symbols). The dotted lines give the corresponding average values for the ridge structures. The analysis was performed on spectra with 4 keV/channel resolution.

sharper ridges are seen in the SD-gated spectra, with FWHM ≈ 13 keV. This is quite close to the case of ^{194}Hg , although the analysis of the fluctuations gives a much smaller number of bands, as discussed in the following section. It is worth noting that the present analysis has been performed on spectra with rather low energy resolution (4 keV/channel), therefore narrower structures (as might be in the case of ^{196}Pb) might be difficult to be precisely measured.

B. Fluctuation analysis

Quantitative information on the average properties of the γ -decay flow can be obtained from the analysis of the fluctuations in the number of counts measured in the γ -coincidence matrices [4,5]. The fluctuation analysis method (FAM) allows one to estimate the number of decay paths available to the rotating nucleus in the γ decay which samples regions in excitation energy and spin associated with different level densities. A path $i \equiv (i_1, i_2)$ is defined as a given pair of coincident $E2$ transitions ($E_{\gamma_1}, E_{\gamma_2}$), corresponding to a point in the γ - γ plane. In particular, a path can belong to a discrete rotational band, populating the ridge structures, or it can be formed by a pair of damped transitions and lie in the $E_{\gamma_1} = E_{\gamma_2}$ valley region. By estimating the number of paths in these two different regions of the spectrum, one can learn about the properties of the rotational structures underlying the γ -decay flow, such as the density of states, the onset of damping, the fragmentation of the $B(E2)$ strength and, in the case of SD nuclei, the probability to decay toward ND states. The number $N_{\text{path}}^{(2)}$ of paths is defined as the weighted average $1/(\sum_i W_i^2)$, where W_i is the probability to follow path i . As a consequence, $N_{\text{path}}^{(2)}$ is strongly affected by the relative population probability, and therefore it strictly corresponds to the real number of paths only when all paths are equally probable, namely, when $W_i = 1/N_{\text{path}}^{(2)}$.

The number of effective paths can be obtained from the experimental spectra using the simple expression

$$N_{\text{path}}^{(2)} = \frac{N_{\text{eve}}}{\frac{\mu_2}{\mu_1} - 1} \times P^{(2)}, \quad (1)$$

where N_{eve} is the number of events, while μ_1 and μ_2 are the first and second moments of the distribution of counts evaluated by the code STATFIT [5] over a sector $\frac{4\hbar^2}{J^{(2)}} \times \frac{4\hbar^2}{J^{(2)}}$ wide ($\frac{4\hbar^2}{J^{(2)}}$ being the average distance between consecutive rotational transitions), in a selected area of the γ - γ spectrum. The superscript (2) indicates that the extraction of the number of paths is based on first and second moments, while the $P^{(2)}$ factor corrects for the finite resolution of the detector system.

The analysis has been carried out for the region of the 1st and 2nd ridges in the Total and ROT-plane spectra (giving information about discrete rotational bands two steps and three steps long, cf. Fig. 1) and for the 1st ridge of the SD-gated spectrum. Known discrete lines, shown by dark areas in Figs. 2 and 3, have been previously subtracted, since they would otherwise dominate the spectrum fluctuations. Figure 8 shows by symbols the results obtained for ^{151}Tb and ^{196}Pb , and by dotted lines the corresponding average values. In both, nuclei up to 30 SD discrete bands are found to populate the total ridges [(a) and (b)], with a gradual decrease at low spins. This is attributed to the decay toward ND states, as previously observed in the analysis of the SD nucleus ^{143}Eu [2]. In addition, the analysis of the 2nd ridge [(c) and (d)] shows that roughly half of these bands extend at least over three consecutive transitions. Only a fraction of the total number of discrete excited SD bands is found to feed into the SD yrast, as follows from the study of the SD-gated ridges [(e) and (f)], in agreement with the previous analysis of the intensities of

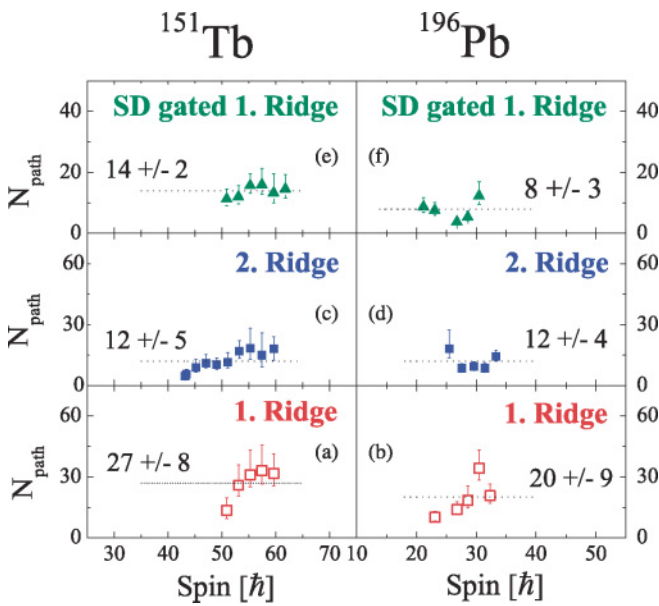


FIG. 8. (Color online) Number of discrete excited SD bands obtained from the experimental analysis of the count fluctuations of ^{151}Tb and ^{196}Pb . Panels (a), (b) and (c), (d) refer to the 1st and 2nd ridges, while (e), (f) to the SD-gated 1st ridges. The dotted lines show the corresponding average values, given by labels.

the ridge structures. The dotted lines give the average values in each case.

IV. INTERPRETATION OF THE DATA

The experimental results, both concerning the intensities and effective number of paths, have been interpreted using a new version of the MONTESTELLA Monte Carlo simulation of the γ -decay flow of ^{151}Tb and ^{196}Pb , which will be discussed in detail in the Part II [31]. The code treats the γ decay within two potentials (i.e., the ND and SD wells), based on the competition between $E2$ collective and $E1$ statistical transitions in both minima [47] and on a tunneling probability across the barrier separating the normal and superdeformed configurations [20], calculated according to the equations of Ref. [48]. The MONTESTELLA code has the unique feature of being based, in the SD well, on energy levels, $E2$ transition probabilities, and potential barriers microscopically calculated by the cranked shell model of Refs. [11,26]. Compared to other Monte Carlo simulations [2,3], this code requires a significantly reduced number of parameters. In addition, it allows one to perform a meaningful fluctuation analysis of the simulated cascades and a selective study of decay paths feeding specific rotational bands, such as the SD yrast.

Using the Monte Carlo simulation one obtains predictions for all the experimental quantities shown in Figs. 4 and 8, i.e., the intensities and fluctuations of the various SD components including, for the first time, the intensity and number of discrete bands in coincidence with the SD yrast. The latter quantities, in particular, can be predicted only via a simulation of the decay flow.

The Monte Carlo simulation is started from an entry distribution in spin and excitation energy which has to be carefully evaluated case by case. Such a distribution could not be measured in the Euroball experiments analyzed here, since the BGO inner ball was not properly calibrated in multiplicity and sum energy. Therefore we have calculated the entry distribution of ^{151}Tb and ^{196}Pb in two steps, as discussed in detail in the Part II [31]: (i) the fusion cross sections of the compound nuclei (CN) ^{157}Tb and ^{200}Pb have been determined, according to the heavy ion reaction model of Ref. [49]; (ii) the final residue distribution has been obtained, as a function of spin I and excitation energy U , by simulating the light particle evaporation by the Monte Carlo version of the code CASCADE [50]. The resulting entry distributions of ^{151}Tb and ^{196}Pb , corrected for the experimental multiplicity requirement, correspond to Gaussian-shaped distributions with a maximum at $I \approx 60$ and $42\hbar$ and $U = 8.3$ and 7.7 MeV, and the full width at half maximum (FWHM) in U equal to 4.3 and 4.7 MeV, respectively.

For both ^{151}Tb and ^{196}Pb , the results of the simulations (based on about 10^6 cascades) reproduce rather well the line shape of the γ spectrum, both concerning the ridges and the total $E2$ quasi-continuum in coincidence with the SD yrast, as shown in the right columns of Figs. 2 and 3. In addition, the superdeformed yrast pattern and the total population of the discrete excited bands forming the 1st and 2nd ridge [dashed lines in Figs. 9(a)–9(d)] are also well accounted for. This requires the adjustment of a limited number of parameters: as discussed in Sec. V B [see also Eqs. (4) and (5) of Part II [31]],

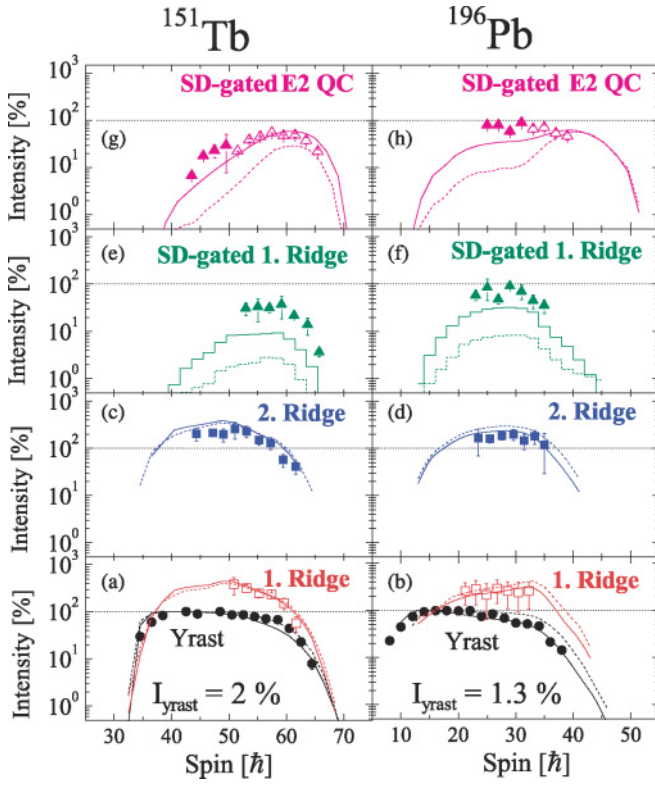


FIG. 9. (Color online) Population of the excited rotational bands in the SD well of ^{151}Tb and ^{196}Pb , relative to the corresponding SD yrast intensity. Data are shown by symbols, consistent with Fig. 4, for the intensities of the SD yrast, the 1st and 2nd ridge, the SD-gated 1st ridges, and the SD-gated $E2$ QC. In (g) and (h), the full symbols refer to data partially contaminated by $M1$'s. Predictions from simulations of the γ decay assuming a standard (enhanced) $E1$ strength (cf. Fig. 10) are shown by dashed (solid) lines (adapted from Ref. [25]).

the tunneling probability has to be adjusted by multiplying the collective mass M of the system by the factor $C_m = 0.7$ and 2.5 in ^{151}Tb and ^{196}Pb , respectively, in order to reproduce the decay-out spin of the SD bands. In addition, a hindrance factor $h_{E1} \approx 0.08$ and 0.036 is used for the $E1$ decay probability in the SD well, in order to keep the population of the SD yrast at the level of $\approx 2\%$ and 1.3% in ^{151}Tb and ^{196}Pb , as measured experimentally. Such hindrance values are of the same order of magnitude as the ones typically used in the ND well (≈ 0.02) [13], although somewhat larger, as discussed in connection with Eq. (2) of Ref. [31].

The general good agreement between data and simulation gives us confidence in the validity of the entry distribution. In addition, it also supports the general prescription used to describe the dynamics of the γ -decay flow, including the tunneling through the potential barrier, as described in Ref. [48]. On the other hand, the Monte Carlo simulation largely underestimates the intensity of the 1st ridge and $E2$ QC in coincidence with the SD yrast [dashed lines in Figs. 9(e)–9(h)]. These observables, although referring to the warm rotation in the transition region between order and chaos, are in fact very sensitive to the delicate balance between $E2$ and $E1$ transitions at low excitation energy, where specific nuclear structure effects are still very important. This large discrepancy

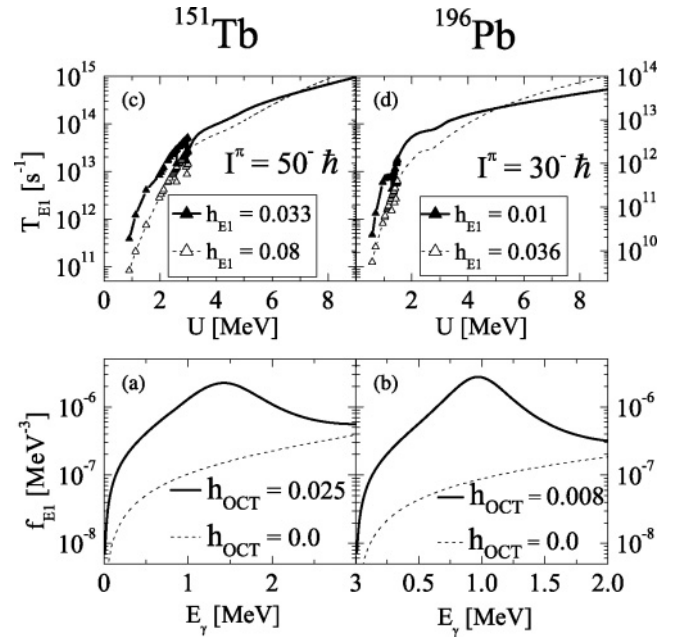


FIG. 10. Panels (a) and (b) show the low energy part of the $E1$ strength function used in the Monte Carlo simulation of ^{151}Tb and ^{196}Pb . Dashed lines refer to the standard f_{GDR} parametrization given by the superposition of three Lorentzian curves, while solid lines are obtained by adding an extra component f_{oct} of Lorentzian shape, with centroid and width $E_{\text{oct}} = 1.5(1.0)$ MeV, $\Gamma_{\text{oct}} = 1.0(0.5)$ MeV and intensity scaled by a factor $h_{\text{oct}} = 0.025(0.008)$. Panels (c) and (d) show the corresponding total T_{E1} decay probability (summed over the three $\Delta I = 0, \pm 1$ components) for negative parity states at spin $I = 50$ and $30\hbar$. The corresponding hindrance factors h_{E1} are given in the legend. Symbols refer to T_{E1} values for the lowest discrete excited states.

seems to point to some peculiarity of the decay probabilities, not included in our model. It is well known that in both $A = 150$ and $A = 190$ mass regions, octupole vibrations play a role in the low-lying excited states of SD nuclei. In fact, as reported in the case of ^{152}Dy [51], ^{196}Pb [52], and ^{190}Hg [53], strongly enhanced $E1$ transitions are experimentally observed, linking the excited SD bands to yrast. In all cases, the $B(E1)$ values are of the order of 10^{-4} W.u., namely, 1 to 2 orders of magnitude larger than expected from the tail of the GDR, in agreement with various theoretical models [54–56]. We have therefore performed simulation calculations for ^{151}Tb (^{196}Pb) adding a new Lorentzian component f_{oct} to the $E1$ strength, with a peak energy $E_{\text{oct}} = 1.5(1.0)$ MeV and a FWHM $\Gamma_{\text{oct}} = 1.0(0.5)$ MeV, as shown by solid lines in Figs. 10(a) and 10(b). The intensity of such a component has been adjusted so that the total $E1$ strength $f_{E1} = f_{\text{oct}} + f_{\text{GDR}}$ is enhanced by about one order of magnitude around 1–2 MeV, consistent with the experimental evidence. This is obtained by scaling the standard Lorentzian curve f_{oct} , normalized in the same way as f_{GDR} , by the additional factor $h_{\text{oct}} \approx 0.01$.

The modification of the $E1$ strength implies an adjustment of the h_{E1} hindrance factor, in order to keep the population of the SD yrast close to the experimental values found in ^{151}Tb and ^{196}Pb . The new h_{E1} values [entering Eq. (2) of Ref. [31]]

for the $E1$ decay in the SD well are now more similar to the value 0.02 used for the ND case [13], being $h_{E1} = 0.033$ and 0.01, respectively. This leads to an effective enhancement of the total $E1$ decay probability T_{E1} , summed over the three $\Delta I = 0, \pm 1$ components, of a factor ≈ 5 for the discrete levels below $U \approx 3$ MeV, as shown in Figs. 10(c) and 10(d). The new simulated spectra are in much better agreement with the data for all quantities, including also the intensities of the ridge and $E2$ QC in coincidence with the SD yrast, as shown by solid lines in Fig. 9 (see also discussion in Sec. III of Part II [31]).

One may speculate that some enhancement effect has to be expected for transitions feeding out of the SD bands, in order to become competitive with the extremely large collectivity of the in-band transitions, which tend to keep the flow going along the rotational bands. In the present work, we attribute such an enhancement to $E1$ transitions only, since our Monte Carlo is based on the competition between pure $E1$ and $E2$, and also because of the experimental evidence for octupole vibrations in both mass regions. However, on the basis of the present analysis, one cannot rule out the possibility that other kind of enhanced transitions may be involved, such as, $M1$'s.

Table I summarizes the parameters for the SD well entering the Monte Carlo code which are found to reproduce at best the γ decay of the SD nuclei ^{151}Tb and ^{196}Pb , respectively.

The use of microscopic levels and decay probabilities allows a detailed study of the population of the SD discrete excited bands, whose intensities can be compared with the experimental values. As discussed in detail in Ref. [31] (see Figs. 6 and 7), most of the microscopically calculated bands show intensity patterns similar to the SD yrast, characterized by a rather flat plateau followed by a sharp decrease, at low spin. This is due to the decay-out into the low deformation minimum. Figure 11 shows a comparison between the experimental intensities of the known discrete SD bands (histograms) and the intensities (at the plateau) of the microscopically

TABLE I. Summary of the parameters for the SD well entering the Monte Carlo simulation code MONTESTELLA for the ^{151}Tb and ^{196}Pb calculations. Lines 1 and 2 refer to the centroid and FWHM of the spin and excitation energy entry distribution of the γ decay; line 3 to the scaling factor C_m of the collective mass; lines 4 and 5 to the centroid and width of the three Lorentzian components of the GDR strength associated with the SD nucleus (see Fig. 2 of Ref. [31]); line 6 to the centroid and width of the extra (octupole) component of Lorentzian shape, shown in Figs. 10(a) and 10(b); line 7 gives the scaling factor h_{oct} of the intensity of the octupole component; line 8 gives the hindrance factor h_{E1} for the $E1$ decay in the SD well [see Eq. (2) and Sec. III of Ref. [31] for details].

No.	Parameter	^{151}Tb	^{196}Pb
1	I , FWHM (\hbar)	61, 15	41, 16
2	U , FWHM (MeV)	8.3, 4.3	7.7, 4.7
3	C_m	0.7	2.5
4	$E_{\text{GDR},i}$ ($i = 1, 2, 3$) (MeV)	8, 18.7, 18.7	9.8, 14.5, 14.5
5	$\Gamma_{\text{GDR},i}$ ($i = 1, 2, 3$) (MeV)	3, 5.7, 5.6	3, 5, 5
6	$E_{\text{oct}}, \Gamma_{\text{oct}}$ (MeV)	1.5, 1	1.0, 0.5
7	h_{oct}	0.025	0.008
8	h_{E1}^{SD}	0.033	0.01

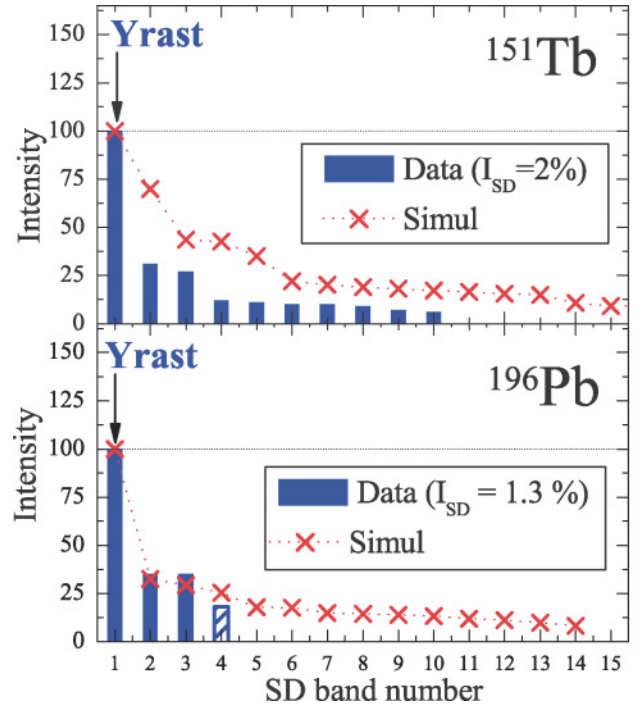


FIG. 11. (Color online) Comparison between the experimental (histogram) and simulated (crosses) relative populations of the strongest SD discrete bands of ^{151}Tb and ^{196}Pb . The intensity of the SD yrast is normalized to 100% and corresponds to ≈ 2 and 1.3% of the γ -decay flux of the corresponding reaction channel. For ^{196}Pb , the experimental intensity of the weakest band (shaded bar) is tentatively assigned [39].

calculated bands (crosses) of ^{151}Tb and ^{196}Pb , as obtained by the MONTESTELLA simulation of the γ -decay flow. The calculations reproduce rather well the general decrease in the population of the excited bands, although in the case of ^{151}Tb the intensity of the excited bands (in particular of the first) is too strong compared to the data. It is worth noticing that such a comparison is qualitative, since no direct correspondence can be established between experimental and simulated bands because of the lack of spin and excitation energy assignment for the excited bands experimentally observed.

The present Monte Carlo simulation can also be used to evaluate the effective number of paths N_{path} , which can be compared with the experimental values reported in Fig. 8. This is possible because the simulation is based on discrete levels, so the fluctuations in the number of events acquire a statistical significance. In fact, as discussed in Sec. III B, the number of paths is defined through the relative population W_i of each path, being $N_{\text{path}} = 1/\sum W_i^2$, therefore such quantity can be evaluated from the calculated intensities of the discrete excited bands, provided that the most intense transitions are excluded as is also done in the data. Equivalently, N_{path} can be extracted from the simulated γ -coincidence spectra (shown in Figs. 2 and 3), after performing (with the STATFIT code [5]) a fluctuation analysis of the event fluctuations. The two approaches are found to provide very similar results.

The number of paths, N_{path} , obtained from the simulation are given by thick solid lines in Fig. 12, for ^{151}Tb and ^{196}Pb ,

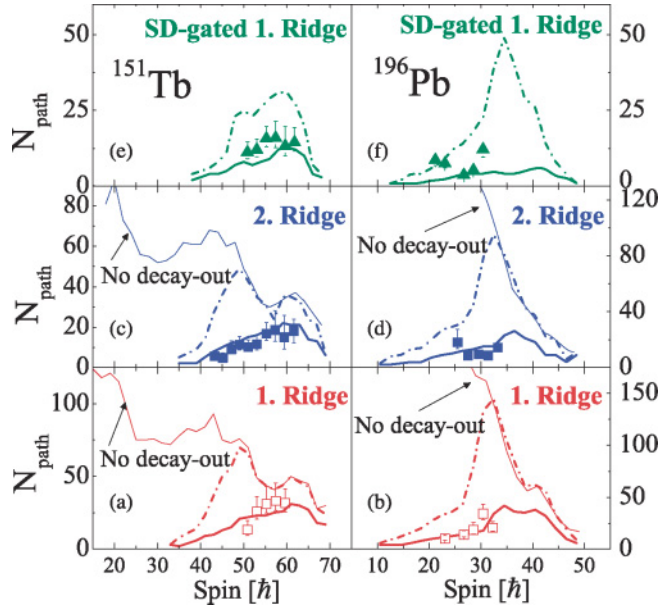


FIG. 12. (Color online) Number of discrete excited SD bands obtained from the analysis of the count fluctuations of the ridge structures of ^{151}Tb and ^{196}Pb . Symbols refer to data, thick solid lines to the Monte Carlo simulation. See the text for the thin and dashed lines.

in the case of the Total 1st ridge, 2nd ridge, and 1st ridge in coincidence with the SD band. This quantity represents a crucial test for various aspects of our model. In fact, N_{path} gives the number of discrete bands that are populated sufficiently strongly, and it is determined by the level density, by the onset of damping (see also the discussion in Sec. IV of Ref. [31]) and by the population mechanism. The latter favors low-lying bands around 1–1.5 MeV, not only because they tunnel less easily through the potential barrier but also because they receive stronger $E1$ feeding. The Monte Carlo calculations provide very good agreement with the data for all three observables over a rather wide range of spin. We also note that the number of paths given by the simulation is much lower than the number N_{band} of discrete bands [defined by the condition $n_b < 2$, see Eq. (6) of Ref. [31]] obtained from the cranked shell model ignoring the flow (thin solid lines in Fig. 12; see also Fig. 22 of Ref. [31]). Taking into account the depopulation of the bands due to the tunneling (as estimated in Ref. [26]) decreases N_{band} at low spins, where the decay-out occurs, but still largely overestimates the data, as shown by dashed lines. This is different from the case of ND nuclei, where discrete bands are found to be more equally populated and N_{path} is closer to N_{band} [13]. For the SD nuclei here discussed, the experimental values can be reproduced only by taking into account the population of the excited bands, which can be obtained on the basis of the Monte Carlo simulation. Figure 13 illustrates the origin of such strong reduction in the measured effective number of paths, as compared to the real number N_{band} . Figures 13(a) and 13(b) show the relative population W_i of all discrete excited bands of the four (π, α) configurations (defined by the condition $n_b < 2$) at spin $I = 40, 50$, and $60\hbar$ in ^{151}Tb and at $I = 20, 30$, and $40\hbar$ in ^{196}Pb . As one can see, the population varies over more than three orders of magnitude,

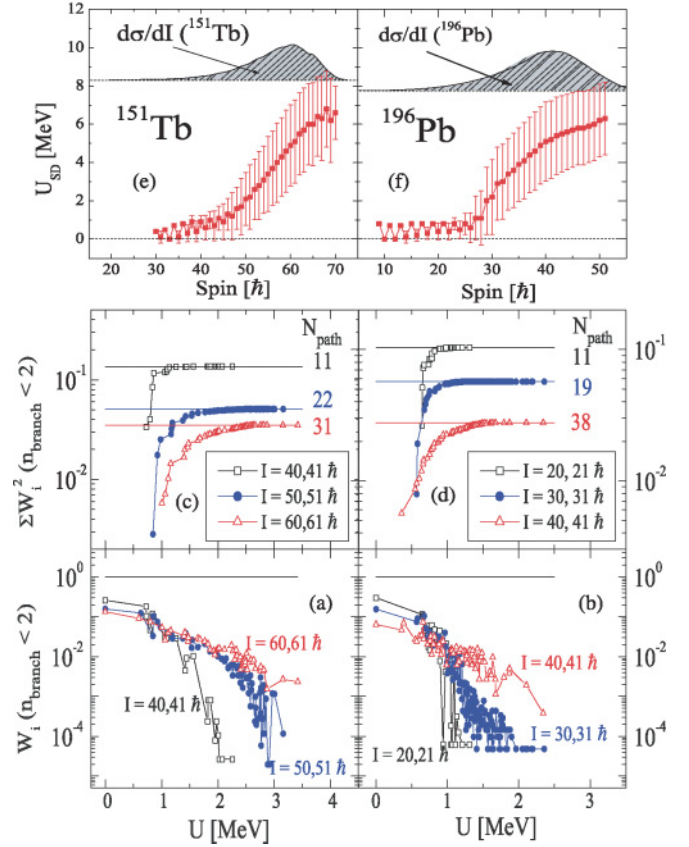


FIG. 13. (Color online) Panels (a) and (b) show the relative population W_i of the discrete excited bands (defined by the condition $n_b < 2$) obtained by the MONTSTELLA simulation at $I = 40, 50, 60\hbar$ in ^{151}Tb and $I = 20, 30, 40\hbar$ in ^{196}Pb . Panels (c) and (d) illustrate the cumulative contribution to $\sum W_i^2$ progressively given by the discrete excited bands, until the full value $1/N_{\text{path}}$ is reached (solid lines). Panels (e) and (f) show the corresponding average internal energy U_{SD} of the decay flow in the SD well as a function of spin, for simulations of the γ decay started from the differential cross sections given in the same panels by shaded areas (see text for details).

being very intense for the lowest lying bands, due to the rapid focusing of the γ -decay flow into the low excitation energy region above the SD yrast. This is illustrated in the top panels of Fig. 13, where the average internal energy U_{SD} for the γ cascades in the SD well is shown for simulation calculations of ^{151}Tb and ^{196}Pb , starting from the corresponding differential cross sections also shown in Figs. 13(e) and 13(f). As a consequence, the corresponding number of paths is determined by the coldest bands with intensities $W_i > 0.01$, as shown in Figs. 13(c) and 13(d), which account for more than 90% of $\sum W_i^2 = 1/N_{\text{path}}$ (solid lines), while the numerous weak bands at higher excitation energies give almost no contribution to the final effective number of paths.

V. PROBES OF TWO-BODY RESIDUAL INTERACTION AND TUNNELING PROCESS

The experimental observables discussed in this work represent a specific test for the physical processes which govern

the rotational motion of strongly deformed nuclei at finite temperature. In fact, the simulated intensities and fluctuations can be used to probe two key ingredients: (i) the strength of the two-body residual interaction which strongly affects the description of nuclear structure at finite temperature [4,13], and (ii) the tunneling probability between the SD and ND well, which strongly depends on the microscopically calculated barriers and collective mass of the system, i.e., on the action S inserted into our simulation code (as discussed in detail in Sec. II of Part II [31]).

A. Sensitivity to the strength of the two-body residual interaction

As discussed in several works on both normal and superdeformed nuclei [8,9,57], a key ingredient in the description of warm rotating nuclei is the two-body residual interaction. This interaction mixes the mean-field configurations, giving rise to a fragmentation of the $E2$ strength with increasing excitation energy (i.e., to the damping of rotational motion), and to a transition into a chaotic regime (see also Sec. IV of Part II [31]). The type and strength of the two-body force have been shown to be crucial for the manifestation of both mixing and damping phenomena: the surface and volume delta interactions produce reasonable overall features of the onset of rotational damping and of the chaotic regime, at variance from other types of interactions (such as the pairing plus quadrupole) [8,57].

In the case of ND nuclei of the rare earth region, it was found [42] that the experimental determination of the number of discrete bands as a function of the length of the rotational cascades, as follows from the analysis of the 1st, 2nd, and higher order ridge structures from γ -coincidence matrices, is very sensitive to the strength of the two-body force. To perform a similar kind of analysis on the superdeformed nuclei ^{151}Tb and ^{196}Pb , we produced two new sets of band mixing calculations, multiplying the interaction strength v_T (see Sec. IV of Ref. [31]) by a factor 1.5 or 0.5. The new sets of energy levels and $E2$ transition probabilities have been used as input for new Monte Carlo simulations of the γ cascades, leaving all other quantities (see Table I) practically unchanged. Only a slight adjustment of the hindrance factor h_{E1}^{SD} has been introduced to keep the same intensity for the SD yrast band. Figures 14 and 15 show the number N_{band} of calculated discrete SD bands [defined by the condition $n_b < 2$, see. Eq. (6) of Ref. [31]] together with the number of paths N_{path} populating the 1st and 2nd ridge structures, as obtained from the ^{151}Tb and ^{196}Pb simulations in comparison with the data. While N_{band} is very sensitive to the strength of the interaction, being roughly inversely proportional to it (as shown by thin lines), N_{path} is much more constant (thick solid lines).

As previously discussed in connection with Figs. 12 and 13, the effective number of paths is largely reduced compared to the number of discrete bands, as a consequence of the large differences in the population probabilities W_i produced by the γ -decay flow which rapidly converges toward low excitation energies above yrast [47]. Only at the highest spin values, namely, above $50\hbar$ in ^{151}Tb and $30\hbar$ in ^{196}Pb , N_{path} shows some dependence on the strength of the two-body force, as clearly shown in Fig. 16. While for ^{196}Pb the present

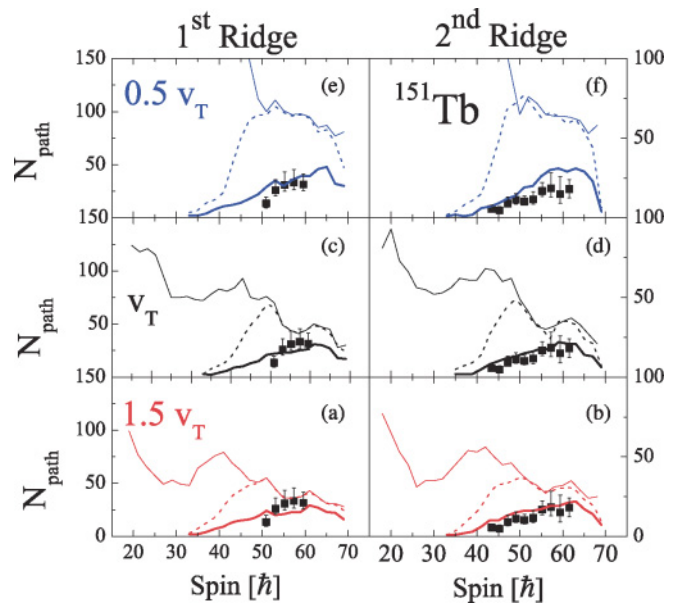


FIG. 14. (Color online) Dependence of the number of discrete excited bands of ^{151}Tb (populating the 1st and 2nd ridges) on the strength of the two-body delta force v_T used in the band mixing calculations. As in Fig. 12, dashed (thin solid) lines give the number N_{band} of discrete bands calculated by the CSM including (or not) the decay-out probability to the ND well. Thick solid lines give the effective number of paths given by the Monte Carlo simulation. Panels (a), (b) correspond to calculations with a factor of 1.5 enhanced strength of the two-body force, panels (c), (d) to a strength with standard values, and panels (e), (f) to a factor of 2 reduced strength. Symbols refer to data (see text for details).

data are outside the range of sensitivity, for ^{151}Tb the more selective analysis of the 2nd ridge [shown in Fig. 16(c)] seems to exclude weaker values of the interaction strength. Note that for ND nuclei, the sensitivity to the interaction strength was only investigated at relatively high spins [42].

B. Sensitivity to the tunneling process

In the present model, the tunneling probability between the SD and ND well is calculated semiclassically and depends on the action S , namely, on the action integral along the tunneling path between the SD and ND wells [see Eqs. (4) and (5) in Ref. [31]]. In particular, S is determined by the height and shape of the potential barrier and by the collective mass M , which is strongly driven by pairing. γ spectroscopy in the quasi-continuum may therefore provide a unique tool for investigating in detail the potential barriers as a function of spin and excitation energy.

The influence of the collective mass associated with the tunneling between the SD and ND wells was investigated in Ref. [26], multiplying the mass M by a factor C_m (see also Ref. [31]). In particular, values of $C_m > 1$ (< 1) will retard (accelerate) the decay-out process, therefore allowing one to fit the spin value at which the decay-out occurs. In the simulation, C_m can be adjusted by fitting the decay-out spin of the yrast SD band, and keeping the same value for all excited SD bands. This leads to very different values for ^{151}Tb and ^{196}Pb : large values

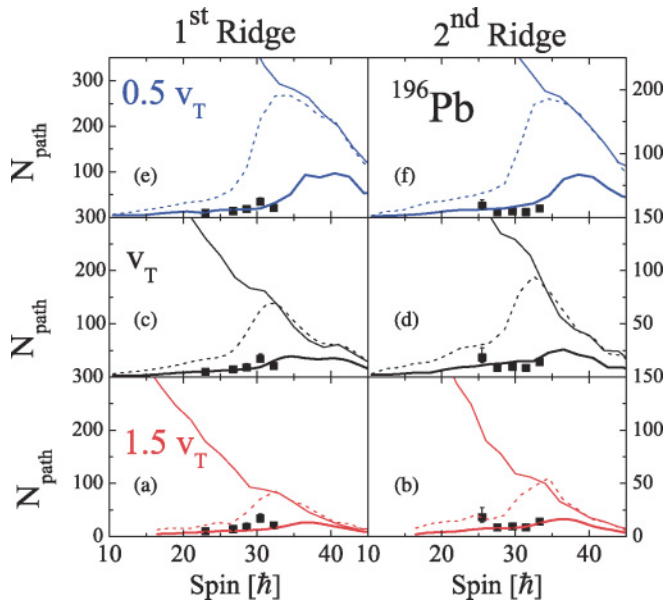


FIG. 15. (Color online) Same as in Fig. 14, but for ^{196}Pb (see text for details).

of $C_m (\approx 2.5)$ are in fact needed to bring the decay-out spin of the SD yrast as low as $\approx 10\hbar$ in ^{196}Pb , while an adjustment of the order of 30% is sufficient to reproduce well the ^{151}Tb case (see Fig. 10 of Ref. [31]). Such values are not specific for these nuclei, but represent instead general features for SD nuclei of $A = 150$ and $A = 190$ mass regions, as follows from the systematic calculations of the intensity of the SD yrast reported in Refs. [26,58].

For ^{196}Pb , the sensitivity to the C_m value has also been tested for the excited SD bands by looking at the intensity and number of paths populating the 1st ridge. As shown in Fig. 17(b), the intensity of the ridge structure is well reproduced by the Monte Carlo calculations using the same $C_m = 2.5$ value found for the SD yrast [Fig. 17(a)], therefore

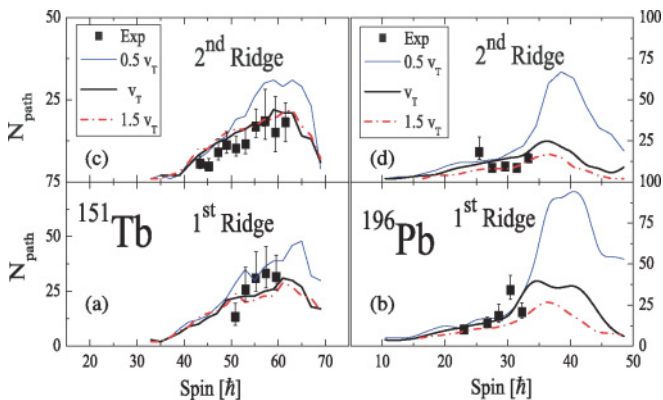


FIG. 16. (Color online) Effective number of paths obtained by Monte Carlo simulations of the γ -decay flow of ^{151}Tb and ^{196}Pb for rotational cascades populating the 1st and 2nd ridges. The simulations are based on three different sets of CSM calculations, obtained by using a standard value of the interaction strength v_T (thick lines), a factor of 2 reduced strength (thin lines), and a factor of 1.5 enhanced strength (dashed lines). Symbols refer to data.

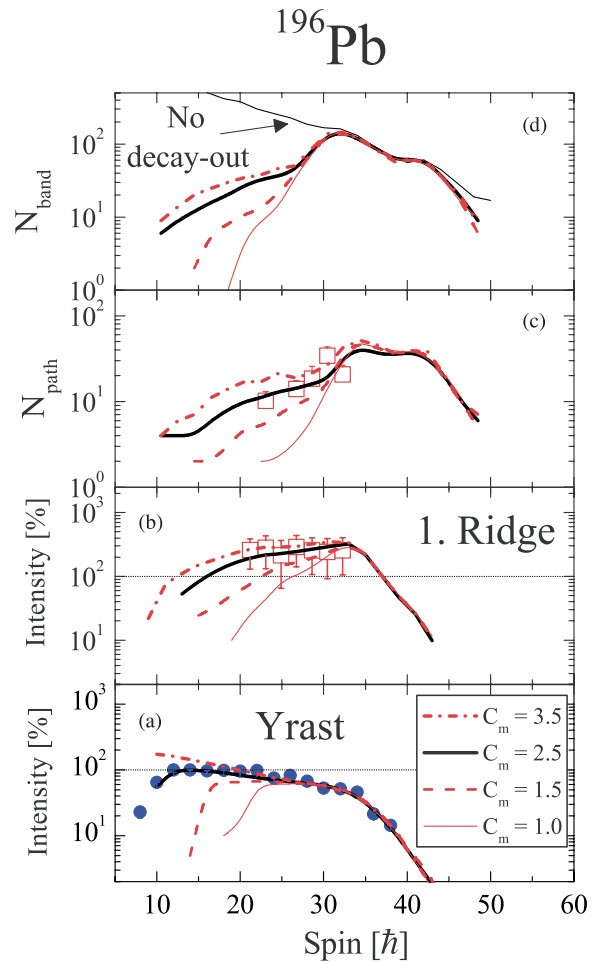


FIG. 17. (Color online) Dependence of the results of the simulation of ^{196}Pb on the scaling factor C_m of the mass parameter. Panels (a) and (b) refer to the intensity of the SD yrast and of the 1st ridge, panel (c) to the number of paths populating the 1st ridge. Panel (d) gives, for the same mass parameters, the number of bands as obtained by the CSM of Ref. [11] (thin solid line), taking also into account the probability to decay-out into the ND well. Symbols refer to the corresponding experimental data (see text for details).

supporting a similar decay-out mechanism for the yrast and the excited bands. The sensitivity to C_m can be further tested by evaluating the number of excited bands: as shown in the top panel of Fig. 17 (and also discussed in Ref. [26] in connection with the calculation for ^{192}Hg) the number N_{band} of excited bands is strongly affected by the probability to decay-out into the ND well, which is regulated by C_m . Even taking into account the strong bias given by the γ -decay flow, which favors the population of the lowest excited bands, the effective number of excited bands (N_{path}) is sensitive to C_m [Fig. 17(c)], showing that values of C_m smaller than 2 lead to unacceptably small intensities and number of paths. This provides, for the first time, a way to test the basic elements of the tunneling process as a function of excitation energy.

Since the decay flow spans the whole range of spin and excitation energies between the yrast line and the entry distribution, the simulations should be sensitive also to the energy and spin dependence of the action S . We note that there

are qualitative differences in the calculated action between the mass $A \approx 150$ and $A \approx 190$ regions. In particular, for a given value of excitation energy, the actions of ^{151}Tb are monotonically increasing as a function of spin. On the contrary, those of ^{196}Pb saturate at $I \approx 20\text{--}30$ or even decrease (cf. Figs. 3 and 4 of Ref. [31]). This is a rather general feature of the mass $A \approx 190$ [26], which reflects the spin dependence of the height of the barrier separating the SD and ND minima. The height decreases at higher spins in the $A \approx 190$ nuclei, while it keeps increasing in most of the cases in the $A \approx 150$ nuclei.

To probe the spin dependence of the actions, we have tried an extreme case, performing Monte Carlo simulations for ^{196}Pb using the actions microscopically calculated for ^{151}Tb , leaving all the other parameters in the simulations unchanged. Doing so, we mainly test the potentials below spin $40\hbar$, where the two sets of calculations are very different. We do not expect to be particularly sensitive at differences at the highest spins, because of the rather low spin entry distribution of ^{196}Pb . The results are shown in Fig. 18 for the SD yrast and the 1st and 2nd ridges, in comparison with standard calculations for ^{196}Pb (thick solid lines). As one can see, the intensities of the yrast and of the 1st and 2nd ridges are strongly distorted, both in their absolute values and in their spin dependences. In particular, the intensities of the ridges tend to become

larger around spin 30, and then decrease much faster, in strong disagreement with the data. Changing the absolute value of the ^{151}Tb actions by modifying C_m does not change the main trends, which are therefore due to the dependence of S on energy and spin. This is in keeping with the fact that the actions calculated for ^{151}Tb have a much more marked spin dependence than those for ^{196}Pb , being larger at high spin and smaller at low spin (cf. Figs. 3 and 4 of Ref. [31]). While these tests are admittedly very schematic, they clearly indicate that the study of the excited SD bands give important information on the microscopically calculated potential energy barriers. More generally, γ spectroscopy in the quasi-continuum may offer a unique opportunity to test the basic elements of the many-body microscopic theory for tunneling processes over the entire range of angular momenta and excitation energy.

VI. CONCLUSIONS

We have presented a detailed study of the γ decay of the SD nuclei ^{151}Tb and ^{196}Pb , based on an ensemble of experimental observables (intensities and fluctuations of different structures present in γ -coincident spectra) which provide strong constraints on the dynamics of the γ -decay flow in the SD well. The experimental data have been compared with simulations based on the interacting cranked shell model. In this way, the simulated γ flow populates discrete quantum levels in the SD well, which is essential to comparing fluctuations in simulated and experimental spectra. Also the probability for tunneling between SD and ND wells were calculated microscopically.

The overall agreement between theory and experiment is satisfactory, requiring the adjustment of only a small number of parameters: they are essentially the collective mass parameter for tunneling (especially for ^{196}Pb), which regulates the spin at which the decay-out occurs, and the $E1$ strength, which is mostly affecting the population of the cold rotational bands. In particular, we have found that to reproduce the SD yrast intensities we have to suppress the $E1$ probability obtained with the standard expression for statistical decay. However, we have also found that to reproduce the intensity of the $E2$ strength gated on the SD yrast, the shape of the $E1$ strength has to be changed compared to the standard Lorentzian parametrization of the tail of GDR, introducing a new component in the 1–2 MeV range. The resulting strength in this energy region is in agreement with the observation of enhanced $E1$ discrete transitions close to the yrast line in various SD nuclei of mass $A = 150$ and 190, caused by the coupling with octupole vibrations.

Another interesting result is that the number of discrete bands effectively populated, which is successfully reproduced by the simulation, is much smaller than calculated by the interacting cranked shell model. This is due to the combined effect of the tunneling through the potential barrier which separates the SD and ND well and of the strong dependence on the γ -decay flow, which favors the population of the coldest bands around 1–2 MeV above yrast. Moreover, for the first time, the experimental data are used to test the sensitivity to the basic ingredients of the physical process, such as the strength of the two-body force and the size of the potential

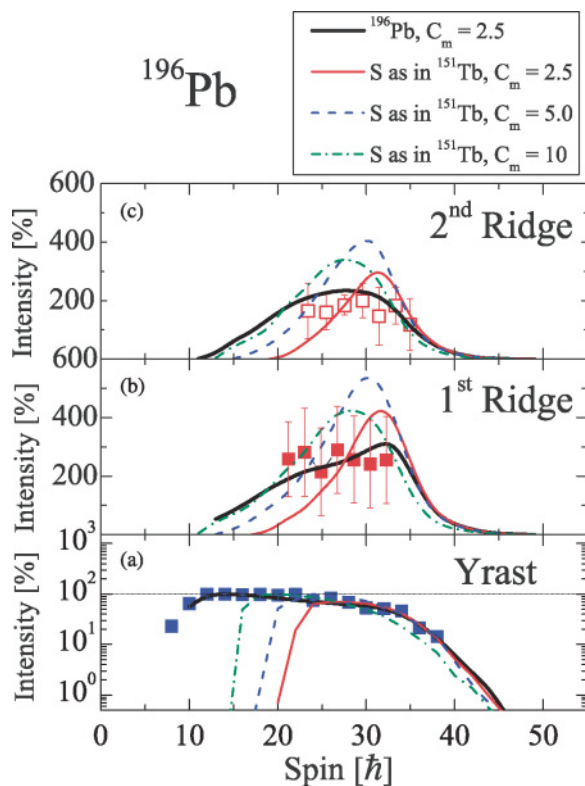


FIG. 18. (Color online) Dependence of the intensity of the SD yrast and 1st and 2nd ridges of ^{196}Pb on the potential barriers separating the SD and ND wells. Solid thick lines refer to the Monte Carlo calculations using the standard parameters for ^{196}Pb (Table I); thin, dashed, and dot-dashed lines give the results obtained using the action S calculated for ^{151}Tb and a collective mass parameter equal to $C_m = 2.5, 5,$ and 10 , respectively (see text for details).

barriers. This is done over the entire range of available spins and excitation energies.

We can then conclude that the study of the warm rotation in the transition region between order and chaos is a very rich playground of interesting physical effects: some are strictly connected to the increasing excitation energy and level density, while others are remnants of processes occurring at low excitations.

ACKNOWLEDGMENTS

The authors thank T. Døssing, T. L. Khoo, and T. Lauritsen for valuable discussions and suggestions. This work was partially supported by the EU (Contract No. EUROVIV: HPRI-CT-1999-00078) and by the Polish Ministry of Science and Higher Education (Grant Nos. 1 P03B 030 030 and N N202 309135).

-
- [1] B. Singh, R. Zywna, and R. B. Firestone, *Nuclear Data Sheets* **97**, 241 (2002).
- [2] S. Leoni *et al.*, *Phys. Lett.* **B498**, 137 (2001).
- [3] T. Lauritsen *et al.*, *Phys. Rev. C* **75**, 064309 (2007).
- [4] A. Bracco and S. Leoni, *Rep. Prog. Phys.* **65**, 299 (2002).
- [5] T. Døssing *et al.*, *Phys. Rep.* **268**, 1 (1996).
- [6] S. Frattini *et al.*, *Phys. Rev. Lett.* **81**, 2659 (1998).
- [7] F. Stephens *et al.*, *Phys. Rev. C* **78**, 034303 (2008).
- [8] M. Matsuo *et al.*, *Nucl. Phys.* **A617**, 1 (1997).
- [9] M. Matsuo *et al.*, *Nucl. Phys.* **A620**, 296 (1997).
- [10] K. Yoshida and M. Matsuo, *Nucl. Phys.* **A612**, 26 (1997).
- [11] K. Yoshida *et al.*, *Nucl. Phys.* **A636**, 169 (1998).
- [12] B. Lauritzen, T. Døssing, and R. A. Broglia, *Nucl. Phys.* **A457**, 61 (1986).
- [13] A. Bracco *et al.*, *Phys. Rev. Lett.* **76**, 4484 (1996).
- [14] M. Matsuo *et al.*, *Phys. Lett.* **B465**, 1 (1999).
- [15] S. Leoni *et al.*, *Phys. Rev. Lett.* **93**, 022501 (2004).
- [16] S. Leoni *et al.*, *Phys. Rev. C* **72**, 034307 (2005).
- [17] G. Benzoni *et al.*, *Phys. Lett.* **B615**, 160 (2005).
- [18] F. S. Stephens *et al.*, *Phys. Rev. Lett.* **94**, 042501 (2005).
- [19] N. Schunck, J. Dudek, and B. Herskind, *Phys. Rev. C* **75**, 054304 (2007).
- [20] E. Vigezzi, R. A. Broglia, and T. Døssing, *Phys. Lett.* **B249**, 163 (1990).
- [21] T. L. Khoo, in *Tunneling in Complex Systems*, edited by S. Tomsovic (World Scientific, Singapore, 1998), p. 229.
- [22] G. Benzoni *et al.*, *Phys. Rev. C* **75**, 047301 (2007).
- [23] S. Leoni *et al.*, *Phys. Lett.* **B409**, 71 (1997).
- [24] A. Lopez-Martens *et al.*, *Phys. Rev. Lett.* **100**, 102501 (2008).
- [25] S. Leoni *et al.*, *Phys. Rev. Lett.* **101**, 142502 (2008).
- [26] K. Yoshida *et al.*, *Nucl. Phys.* **A696**, 85 (2001).
- [27] E. Melby *et al.*, *Phys. Rev. Lett.* **83**, 3150 (1999).
- [28] A. C. Larsen *et al.*, *Phys. Rev. C* **76**, 044303 (2007).
- [29] A. Zilges *et al.*, *Phys. Lett.* **B542**, 43 (2002).
- [30] N. Paar *et al.*, *Rep. Prog. Phys.* **70**, 691 (2007).
- [31] S. Leoni *et al.*, *Phys. Rev. C* **79**, 064307 (2009).
- [32] J. Simpson, *Z. Phys. A* **358**, 139 (1997).
- [33] Achievements with the Euroball Spectrometer, edited by W. Korten and S. Lunardi, 2004, <http://euroball.inl.infn.it/>.
- [34] A. K. Singh *et al.*, *Nucl. Phys.* **A707**, 3 (2002).
- [35] A. K. Singh *et al.*, *Phys. Rev. C* **66**, 064314 (2002).
- [36] C. M. Petrache *et al.*, *Nucl. Phys.* **A579**, 285 (1994).
- [37] G. Duchene *et al.*, *AIP Conf. Proc.* **701**, 222 (2004).
- [38] J. Robin *et al.*, *Phys. Rev. C* **77**, 014308 (2008).
- [39] S. Bouneau *et al.*, *Z. Phys. A* **358**, 179 (1997).
- [40] J. Robin *et al.*, *Phys. Rev. C* **78**, 034319 (2008).
- [41] A. Wilson *et al.*, *Phys. Rev. Lett.* **95**, 182501 (2005).
- [42] S. Leoni *et al.*, *Eur. Phys. J. A* **4**, 229 (1999).
- [43] O. Andersen, J. D. Garrett, G. B. Hagemann, B. Herskind, D. L. Hillis, and L. L. Riedinger, *Phys. Rev. Lett.* **43**, 687 (1979).
- [44] D. C. Radford, *Nucl. Instrum. Methods A* **361**, 297 (1995).
- [45] T. Lauritsen *et al.*, *Phys. Rev. C* **62**, 044316 (2000).
- [46] R. G. Henry *et al.*, *Phys. Rev. Lett.* **73**, 777 (1994).
- [47] T. Døssing and E. Vigezzi, *Nucl. Phys.* **A587**, 13 (1995).
- [48] K. Schiffer *et al.*, *Z. Phys. A* **332**, 17 (1989).
- [49] A. Winther, *Nucl. Phys.* **A594**, 203 (1995).
- [50] F. Pulhofer, *Nucl. Phys.* **A280**, 267 (1977).
- [51] T. Lauritsen *et al.*, *Phys. Rev. Lett.* **89**, 282501 (2002).
- [52] D. Roßbach *et al.*, *Phys. Lett.* **B513**, 9 (2001).
- [53] A. Korichi *et al.*, *Phys. Rev. Lett.* **86**, 2746 (2001).
- [54] J. Kvasil, N. LoIudice, F. Andreozzi, F. Knapp, and A. Porrino, *Phys. Rev. C* **75**, 034306 (2007).
- [55] N. Lo Iudice *et al.* (private communication).
- [56] T. Nakatsukasa *et al.*, *Phys. Lett.* **B343**, 19 (1995).
- [57] M. Matsuo, T. Døssing, E. Vigezzi, and R. A. Broglia, *Phys. Rev. Lett.* **70**, 2694 (1993).
- [58] Y. R. Shimizu, M. Matsuo, and K. Yoshida, *Nucl. Phys.* **A682**, 464c (2001).